THE JOURNAL OF PHYSICAL CHEMISTRY C

Article

pubs.acs.org/JPCC

Insight into the Electrodeposition of Si_xGe_{1-x} Thin Films with Variable Compositions from a Room Temperature Ionic Liquid

Abhishek Lahiri,*[,†] Mark Olschewski,[†] Oliver Höfft,[†] Sherif Zein El Abedin,[†,‡] and Frank Endres*[,†]

[†]Institute of Electrochemistry, Clausthal University of Technology, Arnold Sommerfeld-Str 6, 38678 Clausthal-Zellerfeld, Germany

[‡]Electrochemistry and Corrosion Laboratory, National Research Centre, Dokki, Cairo 12622, Egypt

Supporting Information

ABSTRACT: In this article, we investigated the electrodeposition of Si_xGe_{1-x} from 1-butyl-1-methylpyrrolidinium bis(trifluoromethylsulfonyl)amide containing different molar concentrations of $SiCl_4$ and $GeCl_4$. Upon the deposition of Si_xGe_{1-x} using a 1:1 molar ratio of $SiCl_4$ and $GeCl_4$, a color change of the deposit from red to green was observed during the cyclic voltammetric scan. On increasing the concentration of $SiCl_4$, only a reddish deposit could be seen during cyclic voltammetry. When the concentration of $GeCl_4$ was increased, only a black deposit was obtained. Constant potential electrodeposition showed the formation of Si_xGe_{1-x} with varying proportions of Si to Ge on changing the molar ratio in the solution. To further evaluate the reaction mechanism of the electrodeposition process, in situ UV visible spectroelectrochemistry was performed. From the changes in the UV spectra combined with XPS and SEM observations, a layered growth process has been proposed during the formation of Si_xGe_{1-x}.

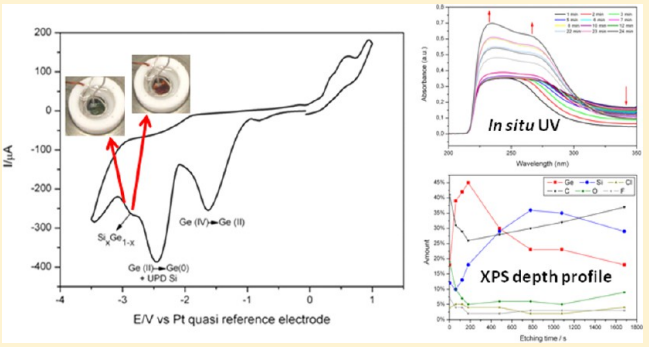

INTRODUCTION

Silicon, germanium, and their compounds have been intensively investigated in the fields of electronics and photonics.[1−4] Semiconductor nanoparticles of these elements show quantum confinement effects, which make such materials interesting for use in opto-electronic devices and quantum computing.[5,6] Silicon and germanium form a continuous series of solid solutions resulting in the formation of Si_xGe_{1-x}. The alloy offers variable crystal lattice parameters and bandgaps, leading to various electrical and optical properties.[7] Recently, in addition it has been shown that both silicon and germanium are excellent anode materials for Li ion batteries and possess quite a high specific capacity.[8]

Thin films of silicon, germanium, and their alloys are mainly synthesized using chemical vapor deposition (CVD), physical vapor deposition (PVD) and molecular beam epitaxy (MBE).[7] A different, low cost approach to develop thin films without the use of vacuum and high temperature is electrodeposition. The viability of electrodeposition of semiconductors from different ionic liquids has already been demonstrated in a number of articles.[9−13] The electrodeposition of germanium and silicon has been studied by in situ scanning tunneling microscopy (STM) and scanning tunneling spectroscopy (STS) techniques.[10] For germanium, an underpotential deposition on Au(111) substrate was reported. STS measurement showed that the bandgap of the deposit was 0.67 ± 0.2 eV.[14] X-ray photoelectron spectroscopy (XPS) was later used to confirm the formation of elemental germanium. For silicon electrodeposition, in situ STM studies showed the formation of silicon islands, and STS studies showed a bandgap of 1.1 ± 0.2 eV, which is consistent with the bandgap of bulk silicon.[10] Electrochemical quartz crystal microbalance (EQCM) analysis showed that the silicon deposition occurs by a four-electron transfer process. However, because of the formation of solvation layers of ionic liquid on the surface, an error in the measurement was noted.[15] Furthermore, in situ Raman spectroscopy indicated the formation of silicon subspecies prior to the reduction process.[16] At present, the reaction mechanism for the electrodeposition of silicon is still not completely understood.

Template-assisted electrodeposition has also been developed to achieve 3DOM and nanowire structures of silicon and germanium.[17,18] The 3DOM structure of both silicon and germanium showed interesting photonic properties. However, because of fast surface oxidation of these semiconductors, characterization of these deposits is not trivial. Silicon nanowires with variable diameters were also achieved by using a polycarbonate template.[19]

The electrodeposition of Si_xGe_{1-x} has been demonstrated.[11] It was shown that during the cyclic voltammetry scan, there was the evolution of colors, which changed from red to orange and green. The change in colors was qualitatively explained with the quantum confinement effect.[11] In situ UV visible spectroscopy studies indicated, however, quite a complicated reaction

Received: August 12, 2013
Revised: November 22, 2013
Published: November 22, 2013

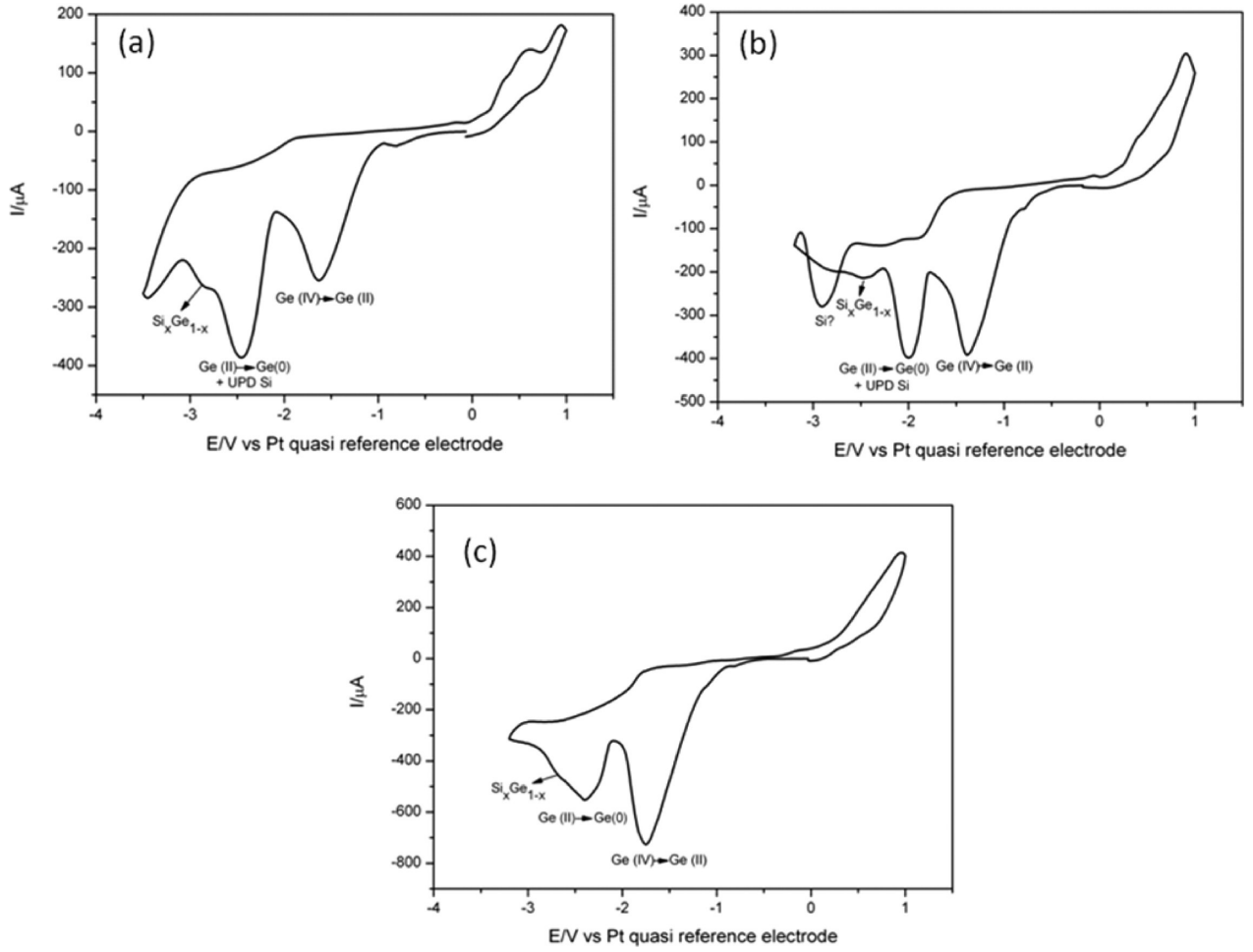

Figure 1. (a) Cyclic voltammogram of 0.1 M $GeCl_4$ + 0.1 M $SiCl_4$ in $[Py_{1,4}]Tf_2N$. The scan rate was 10 mV sec^{-1}. (b) Cyclic voltammogram of 0.1 M $GeCl_4$ + 0.25 M $SiCl_4$ in $[Py_{1,4}]Tf_2N$. (c) Cyclic voltammogram of 0.25 M $GeCl_4$ + 0.1 M $SiCl_4$ in $[Py_{1,4}]Tf_2N$. The substrate was polycrystalline gold, and the temperature was 25 °C.

mechanism.[20] The UV measurements indicated that initially silicon and germanium nanoparticles are formed, which then combine during the electrodeposition process to form Si_xGe_{1-x}. The quantum confinement effect was also confirmed using this technique.[20]

In this article, we describe the influence of changing the molar concentration of both $GeCl_4$ and $SiCl_4$ on the electrodeposition of Si_xGe_{1-x} in 1-butyl-1-methylpyrrolidinium bis(trifluoromethylsulfonyl)amide ($[Py_{1,4}]Tf_2N$). Cyclic voltammetry showed that changing the concentrations of $GeCl_4$ and $SiCl_4$ influences the reduction potential and the formation of Si_xGe_{1-x}. Constant potential electrodeposition was performed to identify the changes in the composition of Si_xGe_{1-x}. The electrodeposit was characterized by scanning electron microscopy (SEM), and the composition was determined using energy dispersive X-ray (EDX) and X-ray photoelectron spectroscopy (XPS). Further evaluation was performed using in situ UV visible spectroelectrochemistry.

EXPERIMENTAL SECTION

1-Butyl-1-methylpyrrolidinium bis(trifluoromethylsulfonyl)-amide ($[Py_{1,4}]Tf_2N$) was purchased in the highest available quality from Io-Li-Tec (Germany) and was used after drying under vacuum at 100 °C to remove the water content to below 2 ppm. $GeCl_4$ (99.999%) was purchased from Alfa Aesar. The working electrode was a sputtered film of gold on glass. The Au substrate was cleaned by refluxing it in isopropanol at 90 °C for 2 h. Prior to the experiments, the gold was carefully heated in a hydrogen flame to reduce any surface contamination. Platinum wires were used as a counter and a quasi reference electrode, which gave good stability in the ionic liquid throughout the experiments. The electrochemical cell was made of Teflon and clamped over a Teflon-covered Viton O-ring onto the substrate, yielding a geometric surface area of 0.3 cm^2. Prior to the experiments, the Teflon cell and the O-ring were cleaned in a mixture of 50:50 vol % of concentrated H_2SO_4 and H_2O_2 (35%) followed by refluxing in distilled water.

The electrochemical measurements were performed in an argon-filled glovebox with water and oxygen contents of below 2 ppm (OMNI-LAB from Vacuum Atmospheres) by using a VersaStat II (Princeton Applied Research) potentiostat/galvanostat controlled by powerCV. The entire scan rate during cyclic voltammetry was 10 mV sec^{-1}. After the constant potential deposition, the deposit was washed in isopropanol and acetone to remove any remaining ionic liquid.

For XPS measurements, the sample was fixed on a molybdenum holder inside of the glovebox and transferred to the UHV using a specialized transfer chamber to avoid any contamination as well as possible. The XPS spectra were obtained using an ultrahigh vacuum (UHV) apparatus with a

dx.doi.org/10.1021/jp408042e | J. Phys. Chem. C 2013, 117, 26070−26076

base pressure below 1×10^{-10} Pa. The sample was irradiated using the Al K alpha line (photon energy of 1486.6 eV) of a nonmonochromatic X-ray source (Omicron DAR 400). Electrons emitted were detected by a hemispherical analyzer (Omicron EA125) under an angle of 45° to the surface normal with a calculated resolution of 0.83 eV for detail spectra and 2.07 eV for survey spectra. All XPS spectra were displayed as a function of the binding energy with respect to the Fermi level.

For quantitative XPS analysis, a Shirley-background-subtraction was employed.[21] Photoelectron peak areas were calculated by fitting Gauss-type profiles optimized by the Levenberg–Marquardt algorithm with the CasaXPS software. Photoelectric cross-sections calculated by Scofield[22] and asymmetry factors calculated by Yeh and Lindau[23] as well as the transmission function of our hemispherical analyzer are taken into account for calculation of stoichiometry. The composition of the sample was given in relation to the deposited layer.

To obtain information on the composition of the underlying layers, the deposit was etched in several steps with argon ions from an Omicron ISE 5 ion source. For this process, argon ions with 2 keV kinetic energy were used resulting in a target current of 20 μA.

In situ spectroelectrochemical experiments were conducted with a Cary 5000 UV–vis–IR spectrometer. The spectroelectrochemical cell was a quartz cuvette (ALS, Japan) having a path length of 0.5 cm. A gold mesh (ALS, Japan) was used as a working electrode. The quartz cell and the gold mesh were cleaned thoroughly in isopropanol and acetone prior to each experiment. Pt wires were used as both reference and counter electrodes and were cleaned in a hydrogen flame. The cell was assembled inside of the Ar filled glovebox. The setup was then introduced into the UV–vis-NIR chamber and connected to the Materials M 510/VersaStat II potentiostat/galvanostat. Argon was continuously passed into the UV–vis chamber during the experiment. A background UV scan was acquired for the electrolyte at open circuit potential and subtracted from consequent measurements with the solutes. UV–vis spectra were measured for any applied potential continuously at a scan rate of 600 nm min^{-1}.

RESULTS AND DISCUSSION

Figure 1a–c shows the cyclic voltammetry curves of 0.1 M $GeCl_4$ + 0.1 M $SiCl_4$ in $[Py_{1,4}]Tf_2N$, 0.1 M $GeCl_4$ + 0.25 M $SiCl_4$ in $[Py_{1,4}]Tf_2N$, and 0.25 M $GeCl_4$ + 0.1 M $SiCl_4$ in $[Py_{1,4}]Tf_2N$, respectively. The saturation concentration of $SiCl_4$ in $[Py_{1,4}]Tf_2N$ is about 1 M.[9] A similar solubility is expected for $GeCl_4$. Therefore, the concentration of both $GeCl_4$ and $SiCl_4$ employed here is lower than the saturation concentration. In the cathodic regime in Figure 1a, we find two prominent reduction peaks at −1.6 and −2.4 V corresponding to the formation of Ge (IV) to Ge (II) species and Ge (II) to Ge (0), respectively. Along with bulk deposition of germanium at −2.4 V, underpotential deposition (UPD) of silicon also takes place. The shoulder at −2.9 V is correlated with the formation of Si_xGe_{1-x}. In the anodic regime, an increase in current was observed above 0.5 V, which could be the partial oxidation of the electrodeposited Si_xGe_{1-x} and of gold.

The CV data in Figure 1a is consistent with the previously published data.[11,20] On increasing the $SiCl_4$ concentration from 0.1 to 0.25 M in the solution, a slight difference in the CV scan was observed, Figure 1b. Again two reduction peaks at −1.4 and −2.0 V were observed in the cathodic direction, which correspond to the Ge (IV) to Ge (II) species and Ge (II) to Ge (0), respectively. However, these peaks are positively shifted compared to those ones in Figure 1a. Also a shoulder peak occurs at −2.5 V. Although the Pt quasi-reversible reference electrode is not a perfect reference electrode for electrochemistry, it is unlikely that the shift in the reduction potential in Figure 1b is due to the shift in the reference electrode as it was shown to be stable over the entire electrochemical window in the case of $GeCl_4$ and $SiCl_4$ in different ionic liquids.[12,24] The shift in the peak and an increase in the reduction current might be related with the complexation of $SiCl_4$/$GeCl_4$ with the ionic liquid, which requires further investigation. When the scan is reversed at −3.2 V, a reduction peak appears at −2.9 V. Such reduction phenomena in the anodic regime have been observed during the electrodeposition of silicon and of Si–Ge alloy and were correlated with the formation of an ionic liquid passivation layer over the electrodeposit.[10,20] The reduction current could be related to the deposition of silicon. On further scanning into the anodic regime, two other reduction shoulders are observed at −2.3 and −1.8 V, which could again be associated with passivation layers. However, these two peaks were not always observed and sometimes converged into one broad peak. The increase in current at above +0.3 V could be related to the partial oxidation of the electrodeposited product and of gold.

When the $GeCl_4$ concentration in the electrolyte is increased from 0.1 to 0.25 M (Figure 1c), the CV again differs from the ones shown in Figure 1a,b. The reduction potential of Ge (IV) to Ge (II) is shifted to −1.8 V. However, the reduction of Ge (II) to Ge (0) occurs at −2.4 V. A small shoulder is observed at −2.6 V. Also, the shoulder is not as prominent as in the cases in Figure 1a,b. In the anodic regime, a current rise is only observed above +0.4 V, which could be correlated with the partial oxidation of the electrodeposited product and of gold.

Furthermore, during the CV scans, colored deposits were obtained during the formation of Si_xGe_{1-x} when the molar concentrations of Ge/Si was 1:1 and 1:2.5. Figures 2 and 3

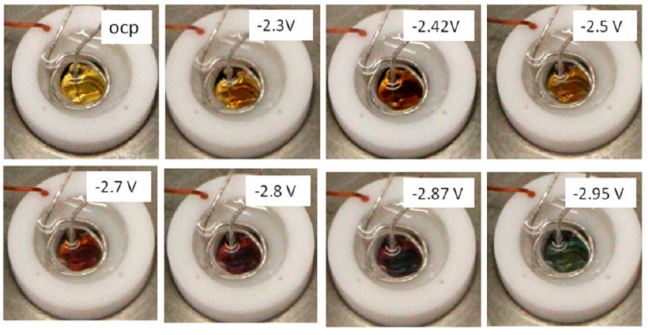

Figure 2. Photographs showing the evolution of colors during the formation of Si_xGe_{1-x} from 0.1 M $GeCl_4$ + 0.1 M $SiCl_4$ in $[Py_{1,4}]Tf_2N$ on polycrystalline gold.

show the color change as a function of electrode potential during the CV scan. As shown in Figure 2, we can see that at open circuit potential (OCP) only the gold substrate is seen. On scanning in the cathodic direction, a reddish deposit starts at −2.3 V and changes to an orange deposit at −2.7 V. The color change from −2.7 to −2.95 V is rapid, and it goes from orange to dark red, to a mixture of red and green, and finally to green.

This observation is consistent with previously reported results.[11] However, on increasing the concentration of $SiCl_4$ to

dx.doi.org/10.1021/jp408042e | J. Phys. Chem. C 2013, 117, 26070–26076

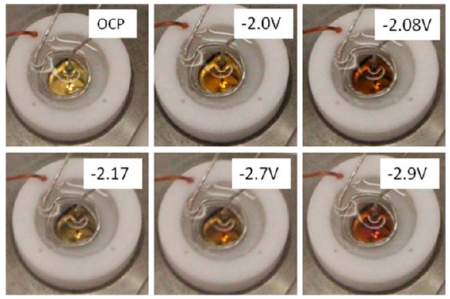

Figure 3. Photographs showing the evolution of colors during the formation of Si_xGe_{1-x} from 0.1 M $GeCl_4$ + 0.25 M $SiCl_4$ in $[Py_{1,4}]Tf_2N$.

0.25 M, mainly the red colored deposit prevailed over the same potential range as seen in Figure 3. For the case of 0.25 M $GeCl_4$ + 0.1 M $SiCl_4$, only a black deposit could be observed in the cathodic regime from −2.3 to −3.2 V. The changes in the deposit color during the deposition of Si_xGe_{1-x} suggest that the dynamics of the process and the nature of the deposit are influenced by changing the $SiCl_4$ and $GeCl_4$ concentrations.

The potentiostatic bulk deposition of Si_xGe_{1-x} alloy was performed at two different potentials from all three electrolyte solutions. Figure 4 shows SEM images of the electrodeposits obtained at −2.5 V. The electrodeposition process was performed for 5 min in order to try to keep the deposit color observed during CV. Figure 4a shows the deposit from 0.1 M $GeCl_4$ + 0.1 M $SiCl_4$ in $[Py_{1,4}]Tf_2N$ at a potential of −2.5 V for 5 min. It is evident that the particles are in the nanometer range with sizes of between 20 and 40 nm. The EDX was performed at five different points, and the average Ge/Si ratio from EDX analysis was found to be about 1.5:1. On increasing the concentration of $SiCl_4$ to 0.25 M and electrodepositing at −2.5 V, the particle size of the deposit increased, agglomerating to clusters, Figure 4b, with particle sizes ranging between 80 and 100 nm. The EDX analysis showed that the Ge/Si ratio was almost 1:1.

Figure 4c shows the microstructure of the electrodeposit from 0.25 M $GeCl_4$ + 0.1 M $SiCl_4$. A clustered morphology is again observed. However, the particle size appears to be about 60−80 nm. The corresponding EDX of Figure 4c is shown in Figure 4d. The Ge/Si ratio was found to be 4:1. Besides Ge and Si, Cl, F, and C peaks are observed, which could be due to the remaining ionic liquid after washing. The oxygen peak is due to the surface oxidation of the deposit during handling outside of the glovebox.

Figure 5 compares the microstructures of Si_xGe_{1-x} formed at −2.8 V. Figure 5a shows the microstructure of Si_xGe_{1-x} from 0.1 M $GeCl_4$ + 0.1 M $SiCl_4$ in $[Py_{1,4}]Tf_2N$. It is evident from the microstructure that very fine nanoparticles are formed, which is consistent with previously reported data.[11]

On increasing the concentration of $SiCl_4$ to 0.25 M, the morphology changes considerably (Figure 5b). A layered type of deposit is obtained. The region marked A shows the morphology of germanium nanoparticles as observed previously in our study.[12] The region marked B seems to have formed on top of the layer A and shows agglomerates made up of small nanoparticles. In comparison, on increasing the concentration of $GeCl_4$ to 0.25 M, we again find the microstructure having a germanium like morphology, Figure 5c. The EDX spectra in Figure 5d represent the Si_xGe_{1-x} obtained from 0.1 M $GeCl_4$ + 0.25 M $SiCl_4$ in $[Py_{1,4}]Tf_2N$. Strong peaks of Si and Ge are observed. Peaks of F, C, and Cl are likely due to the ionic liquid residue, whereas O is from the oxidation of the surface layer during handling outside of the glovebox.

The formation of the layered structure obtained from 0.25 M $SiCl_4$ + 0.1 M $GeCl_4$ in Figure 5b was further studied using

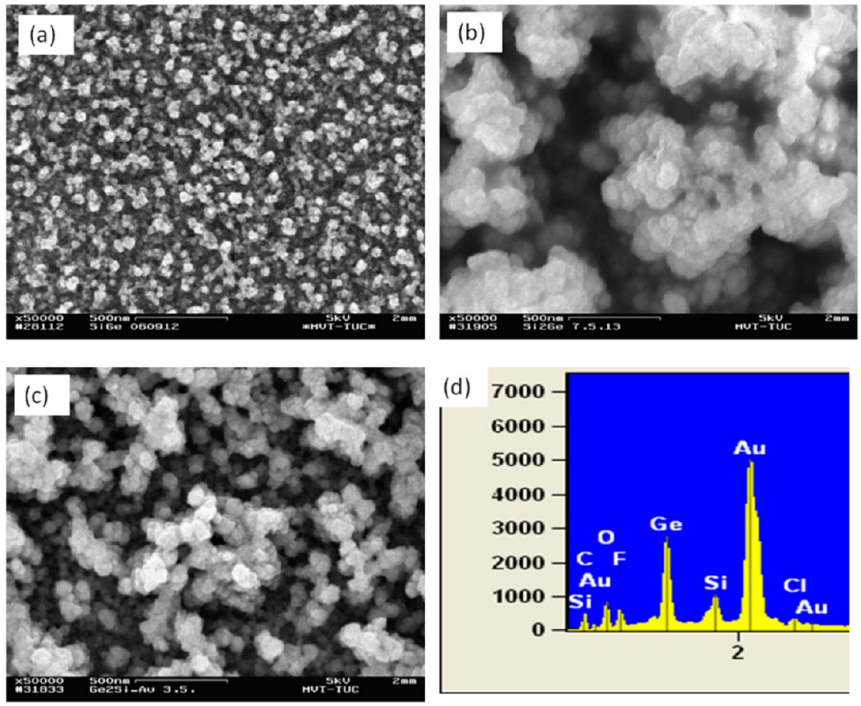

Figure 4. (a) Microstructure of Si_xGe_{1-x} from 0.1 M $GeCl_4$ + 0.1 M $SiCl_4$ in $[Py_{1,4}]Tf_2N$ after 5 min of electrodeposition at a potential of −2.5 V, (b) from 0.1 M $GeCl_4$ + 0.25 M $SiCl_4$ in $[Py_{1,4}]Tf_2N$, and (c) from 0.25 M $GeCl_4$ +0.1 M $SiCl_4$ in $[Py_{1,4}]Tf_2N$; (d) EDX spectra of panel c.

dx.doi.org/10.1021/jp408042e | J. Phys. Chem. C 2013, 117, 26070−26076

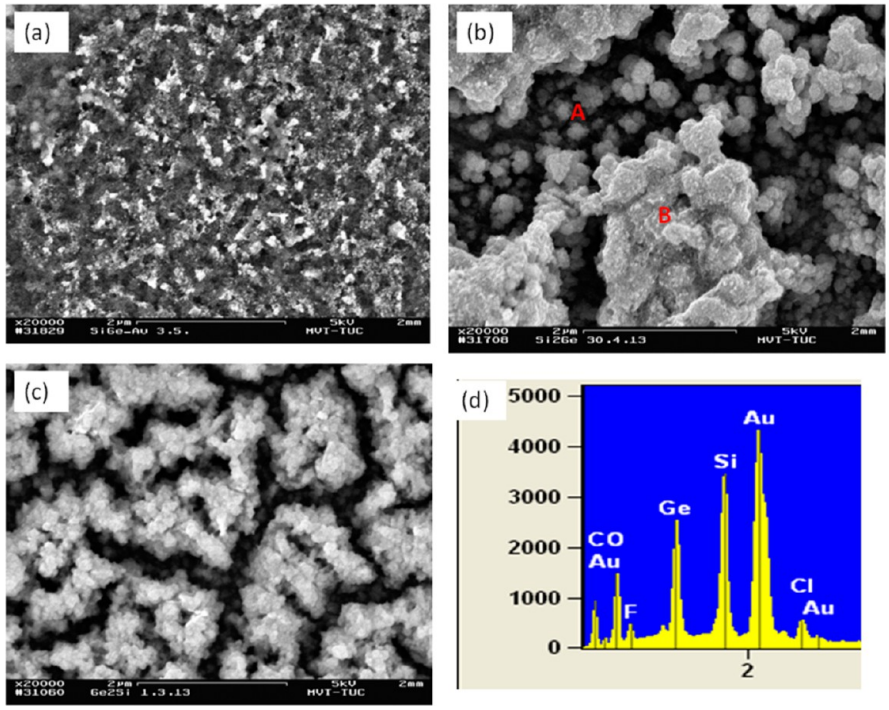

Figure 5. (a) Microstructure of Si_xGe_{1-x} from 0.1 M $GeCl_4$ + 0.1 M $SiCl_4$ in $[Py_{1,4}]Tf_2N$ after 5 min of electrodeposition at −2.8 V, (b) from 0.1 M $GeCl_4$ + 0.25 M $SiCl_4$ in $[Py_{1,4}]Tf_2N$, and (c) from 0.25 M $GeCl_4$ + 0.1 M $SiCl_4$ in $[Py_{1,4}]Tf_2N$; (d) EDX spectra of panel b.

XPS. The thickness of the sample was about 250 nm. The depth profile concentrations of silicon and germanium were obtained by etching the sample inside of the XPS chamber with an Ar^+ beam. XPS analysis of the sample surface showed the presence of Si, Ge, and smaller amounts of O, C, Cl, and F owing to surface contamination and surface oxidation (see Supporting Information Figure S1). The concentrations of various elements of the deposit at different etching time are shown in Figure 6.

From Figure 6, it is evident that in the first three minutes of etching, the concentration of Ge increases significantly, whereas the concentrations of F, C, Cl, and O decrease. The F, C, and Cl are due to ionic liquid traces, and O is due to surface oxidation during the transfer of the sample to the XPS chamber. The increase in carbon after three minutes of sputtering might

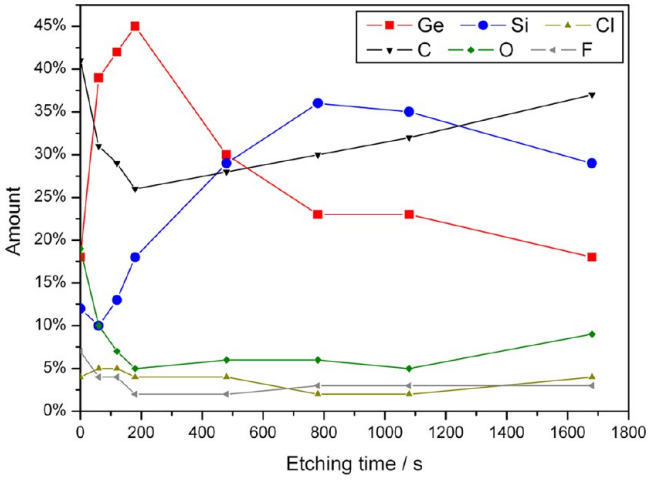

Figure 6. Variation in the concentrations in Ge, Si, C, F, Cl, and O during etching of the Si_xGe_{1-x} electrodeposit with an Ar^+ beam.

be due to the presence of some decomposed ionic liquid during electrodeposition, trapped inside of the porous electrodeposit. An influence of the anodic decomposition product of the ionic liquid at the counter electrode on the Si_xGe_{1-x} electrodeposit has been shown previously, wherein the electrodeposit was shown even to redissolve in the ionic liquid.[25] An XPS analysis of germanium and silicon individually deposited from the same ionic liquid did not show such an effect. Further analysis is needed to ascertain the exact reason for the increase of carbon in the case of Si_xGe_{1-x}. The XPS depth profile analysis of silicon in Figure 6 showed that there is a decrease in the concentration in the first two minutes of etching, after which there is a continuous increase in concentration with etching time. The increase in germanium concentration with etching could be related to the formation of the underlayer as observed in Figure 5b (marked A). However, on increasing the etching time beyond three minutes, the concentration of germanium decreases and silicon increases until it almost plateaus after 10 min. This indicates that during initial deposition a Si_xGe_{1-x} layer is formed with higher concentration of silicon. Furthermore, the change in the concentrations of silicon and germanium with etching time indicates that the kinetics of the reaction changes during the electrodeposition process.

To evaluate further the formation of Si_xGe_{1-x} and the evolution of colors during CV, in situ UV visible spectroelectrochemistry was performed. Figure 7 compares the UV absorption spectra from the three different electrolytes at a deposition potential of −2.8 V. Figure 7a represents the overall UV−visible spectra during the deposition of Si_xGe_{1-x} from 0.1 M $GeCl_4$ + 0.1 M $SiCl_4$. A detailed in situ UV visible spectroscopic study has already been shown in our previous paper for this system.[20] The salient features in figure 7a are the prominent peaks around 225 and 275 nm. The peak at 225 nm is the formation of Ge^{2+} species.[26] The peak at 275 nm is the direct transition at X in the Brillouin zone for the formation of

dx.doi.org/10.1021/jp408042e | J. Phys. Chem. C 2013, 117, 26070−26076

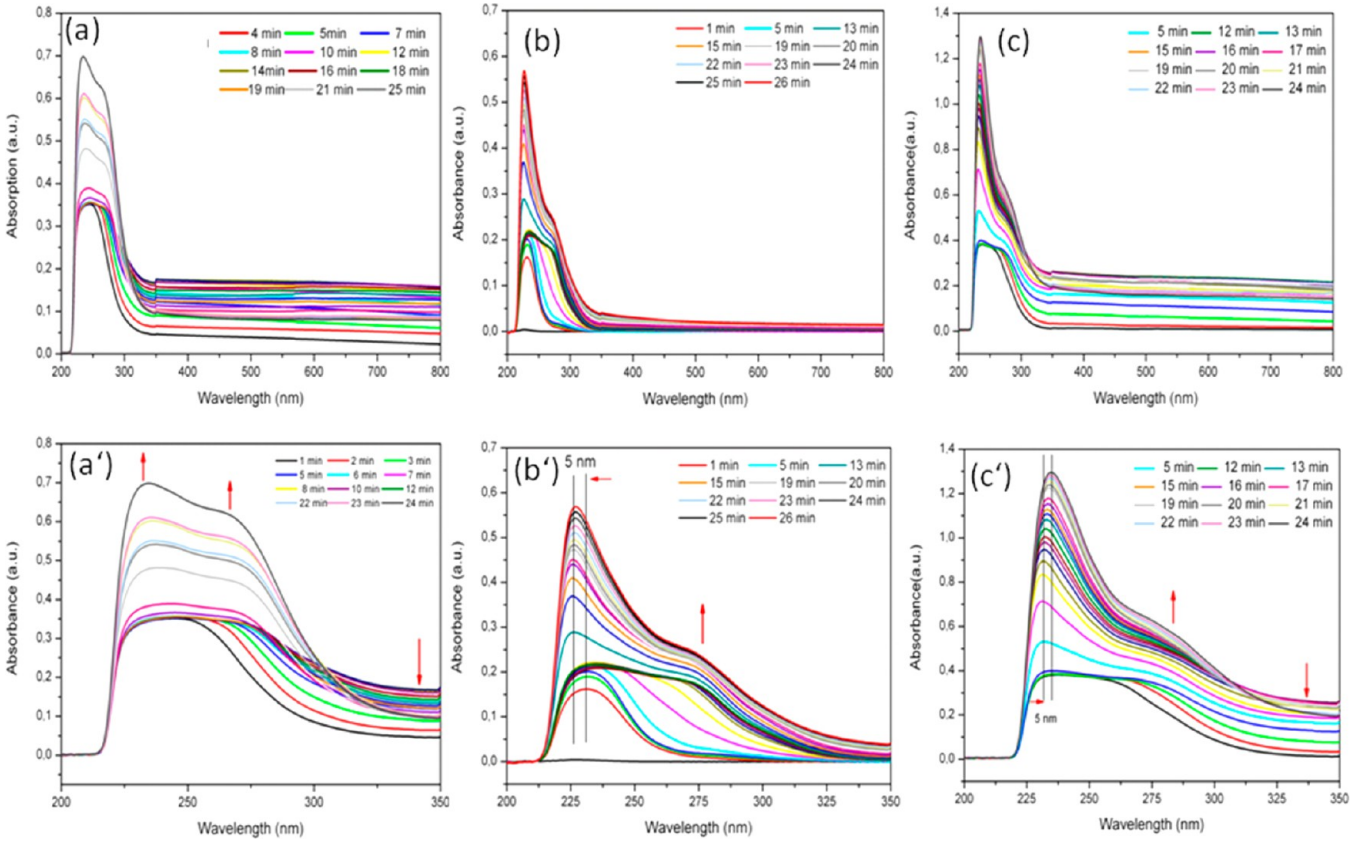

Figure 7. (a) Changes in the UV−visible spectra during the deposition of Si_xGe_{1-x} from 0.1 M $GeCl_4$ + 0.1 M $SiCl_4$ in $[Py_{1,4}]Tf_2N$ at −2.8 V. (a′) Magnified UV−visible spectra of panel a between 200 and 350 nm; (b) from 0.1 M $GeCl_4$ + 0.25 M $SiCl_4$ in $[Py_{1,4}]Tf_2N$ at −2.8 V. (b′) Magnified UV−visible spectra of panel b between 200 and 350 nm; (c) from 0.25 M $GeCl_4$ + 0.1 M $SiCl_4$ in $[Py_{1,4}]Tf_2N$ at −2.8 V. Each spectrum corresponds to one minute of deposition. (c′) Magnified UV−visible spectra of panel c between 200 and 350 nm.

Ge nanoparticles.[27] However, after 7 min of the electrodeposition process, the absorption starts to decrease, which is clearly seen around 350 nm, Figure 7a′, whereas the peaks at 225 and 275 nm increase. Beyond 350 nm, another peak was formed at 595 nm, which blue-shifted by 8 nm (Supporting Information Figure S2). This decrease in absorption and blue shift was assigned to the formation of Si_xGe_{1-x}.[20] On increasing the concentration of $SiCl_4$, the UV spectra show a peak around 227 nm, which increases with time, Figure 7b. No additional peak is formed beyond 350 nm. After 7 min of the electrodeposition, a shoulder peak at 275 nm is observed, which corresponds to the direct transition at X in the Brillouin zone for the formation of Ge nanoparticles, Figure 7b,b′.[27] On continuation of the electrodeposition process to 13 min, a 5 nm blue shift at 227 nm is observed, Figure 7b′. Compared to Figure 7a′, no reduction in the absorption is observed. This blue shift might be due to the formation of silicon-rich Si_xGe_{1-x} layer. For Si nanoparticles, a Γ_{25} to Γ_2' transition in the Brillouin zone occurs at 220 nm,[28] thus indicating the formation of Si-rich Si_xGe_{1-x} during the electrodeposition process.

The UV−vis spectra is supported by the SEM in Figure 5b and XPS in Figure 6, which showed the formation of a layered structure and the formation of a Si-rich Si_xGe_{1-x}, respectively. The UV spectra when electrodepositing from 0.25 M $GeCl_4$ + 0.1 M $SiCl_4$ in $[Py_{1,4}]Tf_2N$ in Figure 7c shows a similar behavior as that in Figure 7a. Initially an increase in absorption is observed and a peak around 226 nm is formed, which could be assigned to the formation of Ge^{2+} species, Figure 7c,c′. A shoulder peak at 275 nm is also observed corresponding to the Brilliouin zone transitions in Ge nanoparticles. After 13 min of the electrodeposition process, the absorption around 350 nm starts to decrease, whereas the shoulder at 275 nm increases (Figure 7c′). Also a red shift of 5 nm around 226 nm is observed. The decrease in absorption around 350 nm and an increase in absorption at 275 nm could be associated with the formation of Ge-rich Si_xGe_{1-x}. The red shift around 226 nm could be the change in the s to p orbital transition in the Ge^{2+} species. In the case of solid matrices such as halides and oxides, it has been shown that the energy of the transitions depend on the metal and its surrounding matrix.[21,29,30] Using the same analogy, we could say that the s to p transition in Ge^{2+} was affected by the presence of Si nanoparticles or subvalent silicon species. However, as the same phenomena is not observed in Figure 7a, it suggests that the kinetics of the reduction process on increasing the $GeCl_4$ concentration is altered giving rise to difference in the energy transitions.

CONCLUSIONS

In this article, we have shown that the concentrations of $SiCl_4$ and $GeCl_4$ in the electrolyte influence the electrodeposition mechanism of Si_xGe_{1-x} from the ionic liquid $[Py_{1,4}]Tf_2N$. During the CV scan in the cathodic regime, colors were noticed, which changed from red to finally green in the case of 0.1 M $GeCl_4$ + 0.1 M $SiCl_4$ in $[Py_{1,4}]Tf_2N$. On increasing the concentration of $SiCl_4$ in the electrolyte, only the red colored deposit was observed, whereas only a black deposit was obtained on increasing the $GeCl_4$ concentration. From constant

dx.doi.org/10.1021/jp408042e | J. Phys. Chem. C 2013, 117, 26070−26076

potential electrodeposition, Si_xGe_{1-x} deposits with varying concentrations of Ge/Si ratio were obtained. The in situ UV visible spectroscopy showed that on increasing the concentration of $SiCl_4$ a blue shift at 227 nm is observed, which could correspond to the formation of Si_xGe_{1-x} with higher silicon content and is consistent with the XPS data. However, on increasing the concentration of $GeCl_4$, a red shift at 225 nm was observed, which could be due to the change in the s to p orbital transition in Ge^{2+} species.

■ ASSOCIATED CONTENT

Supporting Information

XPS and UV−vis spectra. This material is available free of charge via the Internet at http://pubs.acs.org.

■ AUTHOR INFORMATION

Corresponding Authors

*(A.L.) E-mail: abhishek.lahiri@tu-clausthal.de.

*(F.E.) E-mail: frank.endres@tu-clausthal.de.

Notes

The authors declare no competing financial interest.

■ REFERENCES

(1) Paul, D. J. Silicon Germanium Heterostructures in Electronics: The Present and the Future. *Thin Solid Films* **1998**, *321*, 172−180.

(2) Paul, D. J. Silicon-Germanium Strained Layer Materials in Microelectronics. *Adv. Mater.* **1999**, *11*, 191−204.

(3) Michel, J.; Liu, J.; Kimerling, L. C. High Performance Ge-on-Si Photodetectors. *Nat. Photonics* **2010**, *4*, 527−534.

(4) Leuthold, J.; Koos, C.; Freude, W. Nonlinear Silicon Photonics. *Nat. Photonics* **2010**, *4*, 535−544.

(5) Barbagiovanni, E. G.; Lockwood, D. J.; Simpson, P. J.; Goncharova, L. V. Quantum Confinement in Si and Ge Nanostructures. *J. Appl. Phys.* **2012**, *111*, 034307/1−034307/9.

(6) Ladd, T. D.; Jelezko, F.; Laflamme, R.; Nakamura, Y.; Monroe, C.; O'Brien, J. L. Quantum Computers. *Nature* **2010**, *464*, 45−63.

(7) Haller, E. E. Germanium: From Its Discovery to SiGe Devices. *Mater. Sci. Semicond. Process.* **2006**, *9*, 408−422.

(8) Teki, R.; Datta, M. K.; Krishnan, R.; Parker, T. C.; Lu, T.-M.; Kumta, P. N.; Koratkar, N. Nanostructured Silicon Anodes for Lithium Ion Rechargeable Batteries. *Small* **2009**, *5*, 2236−2242.

(9) Zein El Abedin, S.; Borissenko, N.; Endres, F. Electrodeposition of Nanoscale Silicon in a Room Temperature Ionic Liquid. *Electrochem. Commun.* **2004**, *6*, 510−514.

(10) Borisenko, N.; Zein El Abedin, S.; Endres, F. In Situ STM Investigation of Gold Reconstruction and of Silicon Electrodeposition on Au (111) in the Room Temperature Ionic Liquid 1-Butyl-1-methylpyrrolidinium bis (trifluoromethylsulfonyl)imide. *J. Phys. Chem. B* **2006**, *110*, 6250−6256.

(11) Wu, M.; Brooks, N. R.; Schaltin, S.; Binnemans, K.; Fransaer, J. Electrodeposition of Germanium from the Ionic Liquid 1-Butyl-1-methylpyrrolidinium dicynamide. *Phys. Chem. Chem. Phys.* **2013**, *15*, 4955−4964.

(12) Lahiri, A.; Zein El Abedin, S.; Endres, F. UV-Assisted Electrodeposition of Germanium from Air- and Water-Stable Ionic Liquid. *J. Phys. Chem. C* **2012**, *116*, 17739−17745.

(13) Harati, M.; Jia, J.; Giffard, K.; Pellarin, K.; Hewson, C.; Love, D. A.; Lau, W. M.; Ding, Z. One-Pot Electrodeposition, Characterisation and Photoactivity of Stoichiometric Copper Indium Gallium Diselenide (CIGS) Thin Films for Solar Cells. *Phys. Chem. Chem. Phys.* **2010**, *12*, 15282−15290.

(14) Endres, F.; Zein El Abedin, S. Nanoscale Electroeposition of Germanium on Au (111) from an Ionic Liquid: an in Situ STM Study of Phase Formation. *Phys. Chem. Chem. Phys.* **2002**, *4*, 1649−1657.

(15) Komadina, J.; Akiyoshi, T.; Ishibashi, Y.; Fukunaka, Y.; Homma, T. Electrochemical Quartz Crystal Microbalance Study of Si Electrodeposition in Ionic Liquid. *Electrochim. Acta* **2013**, *100*, 236−241.

(16) Nishimura, Y.; Fukunaka, Y.; Miranda, C. R.; Nishida, T.; Nohira, T.; Hagiwara, R. in Situ Raman Spectroscopy Studies of the Electrolyte-Substrate Interface During Electrodeposition of Silicon in a Room-Temperature Ionic Liquid. *ECS Trans.* **2009**, *16*, 1−6.

(17) Meng, X.; Al-Salman, R.; Zhao, J.; Borissenko, N.; Li, Y.; Endres, F. Electrodeposition of 3D Ordered Macroporous Germanium from Ionic Liquids: A Feasible Method to Make Photonic Crystals with a High Dielectric Constant. *Angew. Chem., Int. Ed.* **2009**, *48*, 2703−2707.

(18) Liu, X.; Zhang, Y.; Ge, D.; Zhao, J.; Li, Y.; Endres, F. Three-Dimensionally Ordered Macroporous Silicon Films Made by Electrodeposition from an Ionic Liquid. *Phys. Chem. Chem. Phys.* **2012**, *14*, 5100−5105.

(19) Mallet, J.; Molinari, M.; Martineau, F.; Delavoie, F.; Fricoteaux, P.; Troyon, M. Growth of Silicon Nanowires of Controlled Diameters by Electrodeposition in Ionic Liquid at Room Temperature. *Nano Lett.* **2008**, *8*, 3468−3474.

(20) Lahiri, A.; Olschewski, M.; Höfft, O.; Zein El Abedin, S.; Endres, F. In situ Spectroelectrochemistry Investigation of Ge, Si, and Si_xGe_{1-x} Electrodeposition from an Ionic Liquid. *J. Phys. Chem. C* **2013**, *117*, 1722−1727.

(21) Shirley, D. A. High Resolution X-ray Photoemission Spectrum of the Valence Bands of Gold. *Phys. Rev. B* **1972**, *5*, 4709−4715.

(22) Scofield, J. H. Hartree−Slater Subshell Photoionizion Cross-Sections at 1254 and 1487 eV. *J. Electron Spectrosc. Relat. Phenom.* **1976**, *8*, 129−137.

(23) Yeh, J. J.; Lindau, I. Atomic Subshell Photoionization Cross Sections and Asymmetry Parameters: $1 \ll Z \ll 103$. *At. Data Nucl. Data Tables* **1985**, *32*, 1−155.

(24) Pulletikurthi, G.; Lahiri, A.; Cartsens, T.; Borisenko, N.; Zein El Abedin, S.; Endres, F. Electrodeposition of Silicon from Three Different Ionic Liquids: Possible Influence of the Anion on the Deposition Process. *J. Solid State Electrochem.* **2013**, *17*, 2823−2832.

(25) Al-Salman, R.; Al Zoubi, M.; Endres, F. Evidence for an Influence of an Anodic Decomposition Products of Ionic Liquid on the Electrodeposition of Si_xGe_{1-x} Semiconductor. *J. Mol. Liq.* **2011**, *160*, 114−118.

(26) Nikol, H.; Becht, A.; Vogler, A. Photoluminescence in Ge (II), Tin (II), and Lead (II) Chloride Complexes in Solution. *Inorg. Chem.* **1992**, *31*, 3277−3279.

(27) Wilcoxon, J. P.; Provencio, P. P.; Samara, G. A. Synthesis and Optical Properties of Colloidal Germanium Nanocrystals. *Phys. Rev. B* **2001**, *64*, 035417/1−035417/9.

(28) Wilcoxon, J. P.; Samara, G. A.; Provencio, P. P. Optical and Electronic Properties of Si Nanoclusters Synthesised in Inverse Micelles. *Phys. Rev. B* **1999**, *60*, 2704−2714.

(29) Ranfagni, A.; Mugnai, D.; Bacci, M.; Viliani, G.; Fontana, M. P. The Optical Properties of Thallium-Like Impurities in Alkali-Halide Crystals. *Adv. Phys.* **1983**, *32*, 823−905.

(30) Blasse, G. Luminescence of Inorganic Solids: From Isolated Centres to Concentrated Systems. *Prog. Solid State Chem.* **1988**, *18*, 79−171.